

GT2011-46259

THIN FILM MODELLING FOR AERO-ENGINE BEARING CHAMBERS

C. Wang

H. P. Morvan

S. Hibberd

K. A. Cliffe

University Technology Centre for Gas Turbine Transmission Systems,
University of Nottingham, University Park, Nottingham
NG7 2RD, UK

ABSTRACT

This paper presents a dynamic mathematical model describing the thin film flow in aero-engine bearing chamber. By analyzing the depth averaged continuity equation and momentum equation term by term, the comprehensive physical mechanisms driving thin film flow are revealed. The terms that require extra modeling work are then identified. As a useful first approach, a thin film model based on presumed quadratic velocity profile is adopted. A preliminary study shows that this model can include the main film flow features in aero-engine bearing chamber, whilst maintain simple formulation and work efficiently. Finally, a converging computational strategy is obtained towards the numerical simulation of engine bearing chamber.

INTRODUCTION

Increasing the efficiency of modern gas turbine engines relies on more efficient transmission systems. Bearing chambers contain and channel the oil used for lubrication and cooling purposes and their development is restricted by the constraints of maximum oil temperature and scavenge conditions. Lubricating oil is released into a bearing chamber by an injector or shed from bearings, travelling through chamber inner space and impacting on outer chamber surfaces and typically forming a thin oil film on the chamber wall. The oil film may become thicker as it is collected and removed from a sump, which is usually located at the bottom of chamber. Additionally, oil may be removed, predominantly as droplets, through a vent. Quantitative analysis of the interaction of both air-droplet and air flow with the development of oil film flow on the chamber walls and outlets and their removal at outlets contribute to the design of more efficient bearing chambers. Detailed numerical studies of wall film flow, film flow-core airflow interaction, droplet trajectories and droplet-film flow interaction provide insight into the critical elements specific to an aero-engine configuration. Whilst existing CFD codes are

capable of resolving the main flow features of droplet laden core flow, they must be combined with a specialized film model in an integrated computation to determine oil film and temperature characteristics in response to air flow conditions and droplet release.

Ideally, a comprehensive understanding can be achieved by resolving all the details of air flow, droplets trajectories, film flow and the interface between air and film. Single phase flow and particle laden flow have been well studied and documented, for example in [1]. Numerous methods also have been developed for resolving and tracking multiphase interfaces, e. g. MAC (Marker and Cell) [2]; Volume of Fluid [3]; and more recently the Level-Set method [4]. If sufficiently fine computational meshes are used, all of these methods are able to accurately resolve and track the interface between two phases as part of a CFD domain; in that sense they “explicitly” resolve the interface in the solution domain. In order to capture the details of the interface, a very fine mesh or a large enough number of tracked interface particles are typically needed. This can be computationally costly, in particular where the film thickness is small relative to the domain dimensions or when the interface changes significantly.

In order to formulate a mathematical description of the film accurately and cost-effectively, selected assumptions and simplifications are to be made. The thin-film assumption is arguably the most common, in which film property variations over its depth are averaged. Thin-film equations can be derived from the Navier-Stokes equations, similar in form to shallow water or boundary layer equations. Further simplifications can be made depending on the application; e.g. the geometrical complexity of bearing chambers can be simplified as an annulus if the inner and outer walls are the only dominant components [5, 6]. The computation of what is then a 2D film with the walls that collect the oil is thus greatly simplified. From the viewpoint of a CFD numerical simulation, the thin film is usually treated as a coupled boundary condition for the core air flow. However,

the underlying assumptions built in the various thin film models available in the literature need to be borne in mind as, while they can facilitate the formulation of the governing equations and their numerical computation, they also limit the situations to which the models can be applied. O'Rourke and Amsden designed a popular (as used in the codes KIVA and ANSYS-FLUENT, for example) thin film model for port-injected engines, whereby the Lagrangian trajectory of the oil is maintained. An oil film height is computed as the ratio between the volume of the droplets found in any given wall cell and the cell area [7, 8]. This approach works well when a large number of droplets are considered, as is the case when atomised particles are the main elements entering a film in an internal combustion engine; but limited for the situation in a bearing chamber where droplets are larger and relatively fewer. Bai & Gosman published a thin film model for spray impingement on walls occurring in both Diesel engines and in gasoline engines [9]. Their model is a Eulerian formulation, more general than O'Rourke and Amsden's, and it has some more potential for the application considered here. A first attempt at bearing chamber applications by the Nottingham team [6] oversaw the formulation of an Eulerian model and provided a first tailored CFD solution to the bearing chamber problem, albeit in a sequential manner. More recently Williams [10] investigated the impact of droplets on idealised films.

The present paper aims to eventually build on this experience to provide a more robust and better integrated thin film model. For the most part it can be assumed that the film behaves as a fast flowing film. Several leading models already exist in the literature based on the thin film assumption and are dedicated to bearing chamber issues [5], some are only applicable to simple situations and geometries; other models are more general but untested in the present context [9]. As a preliminary task, the dynamics of thin-film flow, under the bearing chamber specific conditions of oil droplet collection and specified core air interactions are evaluated within a simplified geometry. A model is implemented in MATLAB [11] to provide a rapid evaluation and validation tool for changing whole-chamber conditions and characterise desirable model features.

MATHEMATICAL DESCRIPTION

Governing equations

If the oil film flow is treated as Newtonian, incompressible and isothermal with film velocity \mathbf{u}_f and pressure p_f , then in general coordinates the flow is governed by continuity equation

$$\nabla \cdot \mathbf{u}_f = 0 \quad (1)$$

and Navier-Stokes equations

$$\rho_f \frac{D\mathbf{u}_f}{Dt} = -\nabla p_f + \rho_f \mathbf{g} + \mu_f \nabla \cdot \nabla \mathbf{u}_f \quad (2)$$

In Eqs. (1) and (2), ρ_f and μ_f are the oil density and viscosity respectively; \mathbf{g} is the acceleration due to gravity.

In a typical bearing chamber configuration, the film flow is more readily described through reference to a curvilinear system of coordinates (s, y, x) , where (s, x) are the coordinates parallel to the chamber wall and y is the coordinate perpendicular to the chamber wall. Taking the film surface as $y = h(s, x, t)$, then local to the bearing chamber wall, a film flow configuration is illustrated in Fig. 1.

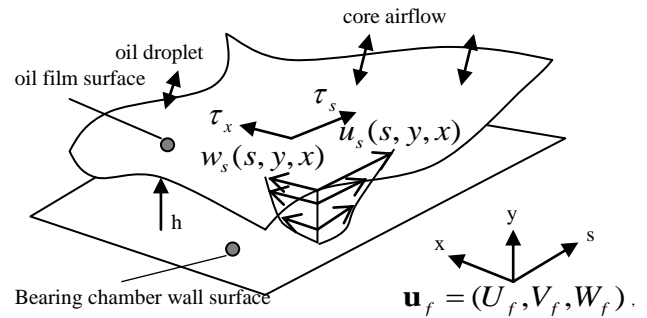


Figure 1. SCHEMATIC OF LOCALIZED OIL FILM ON THE SURFACE OF THE 3D BEARING CHAMBER.

Thin film assumptions

Since the film flow over the surface of the chamber tends to be thin, the depth averaged governing equations are usually used for flow analysis. Here, the depth averaged integration is defined as

$$\bar{\phi}(s, x, t) = \frac{1}{h} \int_0^h \phi(s, y, x, t) dy \quad (3)$$

According to experimental observation in bearing chambers, the typical thickness of film h is usually small compared with the radius of the chamber R , i.e. $\varepsilon = h/R \ll 1$. For fluid flow this restricts the fluid acceleration across the film thickness and the flow is dominated locally by the chamber and the interface conditions. By using non-dimensional analysis, the order linked to ε for each term in governing Eqs. (1) and (2) can be simplified [12]. Keeping the terms with order up to $O(\varepsilon)$ and applying depth averaging integration to continuity Eq. (1), the depth averaged continuity equation can be obtained as

$$\frac{\partial h}{\partial t} + \frac{\partial h \bar{U}_f}{\partial s} + \frac{\partial h \bar{W}_f}{\partial x} = V_f \Big|_{y=0} + \frac{\dot{m}}{\rho_f} \quad (4)$$

The term $V_f \Big|_{y=0}$ in Eq. (4) denotes the contribution of the oil flow at $y=0$. Keeping the terms up to $O(\varepsilon)$ and applying depth averaging integration to Eq. (2), a depth averaged momentum equation can be obtained as

$$C_\xi = E_\xi + G_\xi + A_\xi + W_\xi + D_\xi + V_\xi + S_\xi \quad (5)$$

in which, the subscript ‘ ξ ’ denotes the coordinate direction (s or x in Fig. 1). Equation (5) is the general depth averaged equation governing the momentum transport within film under the thin film approximation. The physical mechanisms driving the transport of $h \bar{U}_f$ in the thin film flow can be categorized as

- *Convection of film,*

$$C_s = \frac{\partial h \bar{U}_f}{\partial t} + \frac{\partial h \bar{U}_f \bar{U}_f}{\partial s} + \frac{\partial h \bar{W}_f \bar{U}_f}{\partial x}$$

- *Variation of velocity profile within the film,*

$$E_s = -\frac{\partial}{\partial s} \int_0^h \hat{U}_f \hat{U}_f dy - \frac{\partial}{\partial x} \int_0^h \hat{W}_f \hat{U}_f dy$$

- *Gravity,*

$$G_s = h \left(\frac{g_y \partial h}{\partial s} + \frac{h \partial g_y}{2 \partial s} + g_s \right)$$

- *Air-film interaction (including pressure and shear stress),*

$$A_s = -h \frac{\partial p_a}{\rho_f \partial s} + \frac{\tau_a}{\rho_f}$$

- *Shear stress from wall,*

$$W_s = \frac{-\tau_w}{\rho_f}$$

- *Droplet-film interaction,*

$$D_s = -\frac{h \partial p_d}{\rho_f \partial s} + \frac{\tau_d}{\rho_f} + \frac{\dot{m} \bar{U}_f}{\rho_f} \Big|_{y=h}$$

- *Flow crossing the wall surface,*

$$V_s = V_f \Big|_{y=0} \bar{U}_f$$

- *Surface tension.*

$$S_s = \frac{h \partial \sigma \kappa_l}{\rho_f \partial s} + \frac{\partial \sigma}{\rho_f \partial s}$$

THIN FILM MODEL FOR A BEARING CHAMBER

The gravity term G_ξ , surface tension term S_ξ and flow extraction term V_ξ are evaluated to include the geometry of wall, surface tension properties and mass flow through the wall. Ideally, if the profile of film velocity is known, the term representing the variation of velocity profile E_ξ and the term representing the contribution of shear stress from wall W_ξ , as described in the previous section, can be evaluated. Unfortunately, the information of velocity profile is filtered by the process of depth averaging; a simple model is provided for the film velocity profile. The remaining information needed to solve Eqs. (4) and (5) are the interaction between air A_ξ and film as well as the interaction between droplet and film D_ξ . The interaction between air and film can be supplied from the computation of the core airflow directly. However, the interaction between droplets and film is complex and excessive computational resource would be needed to capture the details of droplet impingement, such as volume fraction and velocity. Usually, the droplet-film interaction is therefore simulated with recourse to a simplified model as part of thin film model framework.

Model of velocity profile

The velocity profile over the depth is usually assumed as a polynomial [5, 9]. According to previous work [12], the thin film flow in an engine bearing chamber is observed as laminar film flow. Therefore in the present paper, the velocity profile is assumed quadratic for simplicity and, for example, the velocity component U_f may be approximated as $U_f = ay^2 + by + c$. Thus the wall shear term can be evaluated from the assumed velocity profile

$$W_s = \frac{-\tau_w}{\rho_f} = \frac{\tau_d}{2\rho_f} + \frac{1}{2} \frac{\tau_a}{\rho_f} - \frac{3\mu_f \bar{U}_f}{\rho_f h} \quad (6)$$

In Eq. (6), there is an extra contribution due to droplet impingement. For convenience, this term is rearranged and put

into the droplet-film interaction; thus the model for the wall shear term is re-written as

$$W_s = \frac{-\tau_w}{\rho_f} = \frac{1}{2} \frac{\tau_a}{\rho_f} - \frac{3\mu_f \bar{U}_f}{\rho_f h} \quad (7)$$

Model of droplet impingement

For modelling the droplet term in Eq. (5), a schematic of droplet-film interaction process is shown in Fig. 2.

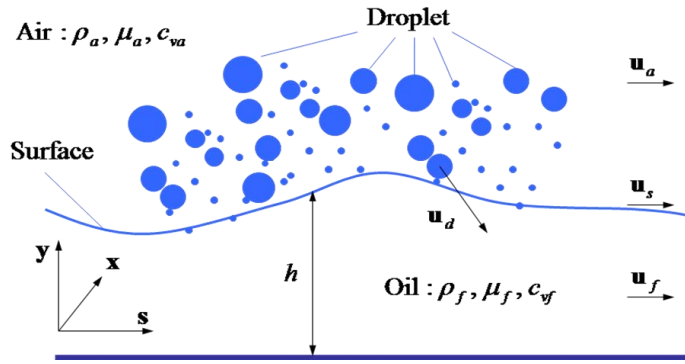


Figure 2. SCHEMATIC OF DROPLETS-FILM INTERACTION.

It is assumed that there are N droplets contacting a unit film area, each with velocity \mathbf{u}_{di} , at one moment. Each droplet contacts film with area ratio α_i . A reasonable assumption is that the density of droplet is the film density ρ_f . When the considered area is reasonably small, the droplet velocity can be considered uniform locally. Also the normal component of film velocity is negligible according to the thin film assumption. Then a simplified droplet-film interaction model may be written as

$$D_s = \frac{h}{\rho_f} \frac{\partial \dot{m} U_{ds}}{\partial s} + \frac{3}{2} \frac{U_{ds}}{\rho_f} \dot{m} - \frac{1}{2} \frac{\bar{U}_f}{\rho_f} \dot{m} \quad (8)$$

Chew's model for bearing chamber

Chew published two thin film models for bearing chamber: one for laminar film flow and one for turbulent film flow [5]. According to previous work [12], the thin film flow in an engine bearing chamber is observed as laminar film flow. In [5],

the laminar velocity profile is assumed as $U_f/\tilde{V} = \eta(2-\eta)$, where $\eta = y/h$. Thus the wall shear term in Chew's model is

$$W_{s,Chew} = \frac{-\tau_w}{\rho_f} = -\frac{3\mu_f \bar{U}_f}{\rho_f h} \quad (9)$$

The droplet impingement is assumed at a uniform rate and so does not include the normal impingement velocity term

$$D_{s,Chew} = \frac{U_{ds}}{\rho_f} \dot{m} \quad (10)$$

In the present paper however, the air-shear term $A_s = \tau_a/\rho_f$ is to be added to Chew's model for the purpose of the calculations we present later

Other simplifications

In Chew's paper, the variation of velocity profile, E_s , was not ignored but it will be in our subsequent calculations, which implies that the depth averaged velocity is assumed to dominant the film transport.

The surface tension term is ignored temporally in the present paper. The effect of this term will be checked in a successor study.

A SIMPLIFIED BEARING CHAMBER

Karlsruhe chamber and simplified geometry

A simplified configuration for an aero-engine is shown in Fig. 3 as a schematic of a bearing chamber rig used for experimental work at the Karlsruhe Institute für Technologie (KIT) [6]. An internal shaft is typically rotating at very high speed and drives the core air flow and air-oil droplet mixture, and possibly further surface interactions. In bearing chambers, sealing pressurized air is commonly used to prevent oil leakage. Relatively cool oil is injected to provide 'heat-to-oil' cooling of walls and bearings to keep them below a critical temperature relevant to minimising oil degradation. All these complex flow features are influenced by the collection, convection and removal of the oil film flow on the wall.

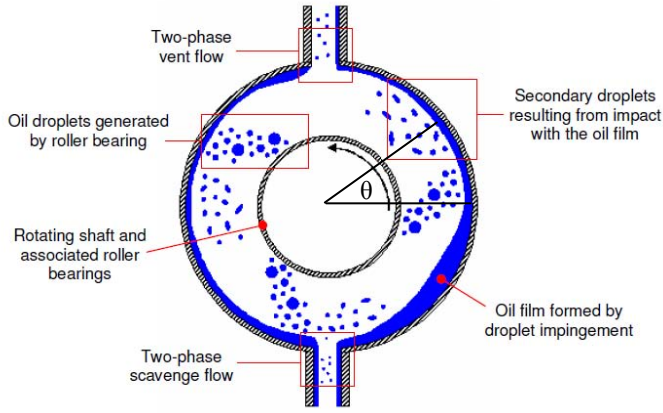


Figure 3. SCHEMATIC OF KARLSRUHE CHAMBER.

The core air flow information needed in depth averaged momentum equation is estimated from a 2D precursor simulation of the air flow between the shaft and chamber outer wall. A mesh with $400 \times N$ cells was used in the computation. The number N here is relative to the shaft rotating speed, and ensures that the nearest cell centre to the wall is within the log-law region. An in-house code based on the finite volume method and Reynolds Averaged N-S equation (RANS) is used and the Launder – Spalding $k - \varepsilon$ model [13] is selected to estimate the Reynolds stress. A wall function is used for dealing with the wall boundary condition.

The shear stress between the air and wall is evaluated for four different shaft rotating speeds and the results are shown in Fig. 4.

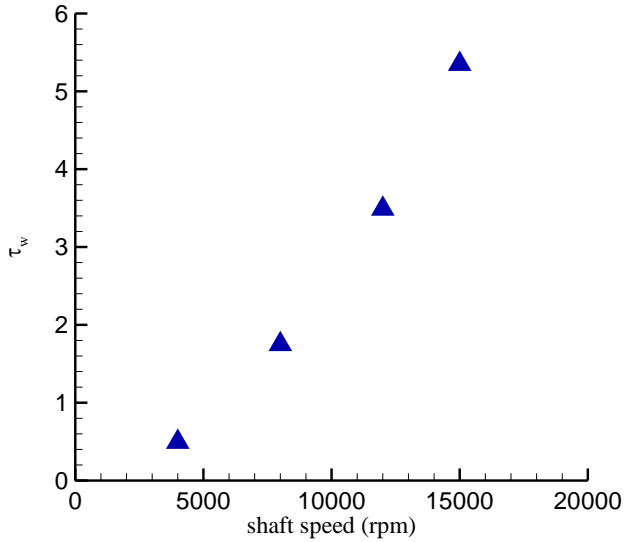


Figure 4. WALL SHEAR STRESS EVALUATED AT SHAFT SPEEDS 4000, 8000, 12000 AND 15000 RPM.

Weak shear driven film flow

With no oil injected into the chamber, the film attached on the outer wall is formed from residual oil and driven by the shear force from the rotating core air flow and balanced by gravitational force and wall friction. The thickness of the film will be limited by the air shear force generated by the rotating speed of the shaft and only for high enough values will exist as a coherent film. Before the droplet-film interaction is studied, the relationship between the shaft speed and the film thickness distribution, when the film is purely driven by core air shear force, is investigated.

From the computational result for the core air flow, it appears that the pressure gradient along the s direction can be neglected. There is no droplet impingement in this case and surface tension is not considered. If the convection of the film flow is very weak, for steady state and with the position of $\theta = 0$ set at 3 o'clock in Fig. 3, the momentum equation along the s direction can be reduced to

$$\mu_f \frac{\partial^2 U_f}{\partial y^2} = \rho_f g \sin\left(\theta + \frac{\pi}{2}\right) \quad (11)$$

After several integral manipulations, the film mass flux can be expressed as

$$q = h\bar{U}_f = \frac{\tau_a}{\mu_f} \frac{h^2}{2} - \frac{\rho_f g \sin(\theta + \pi/2)}{\mu_f} \frac{h^3}{3} \quad (12)$$

By using a depth averaged equation, the equation describing the distribution of film thickness under weak convection is obtained

$$\frac{dh}{d\theta} = \frac{\rho_f g \cos(\theta + \pi/2) \frac{h^2}{3}}{\tau_a - \rho_f g \sin(\theta + \pi/2)h} \quad (13)$$

With a fixed flux $q = h\bar{U}_f$ and τ_a , the film thickness at the bottom of chamber ($\theta = -\pi/2$) can be determined as

$$h_{\theta=-\pi/2} = \sqrt{\frac{2\mu_f q}{\tau_a}} \quad (14)$$

To enable the film to be attached on the wall surface continuously and smoothly, the denominator on the right hand side of Eq. (13) should never be null. A limit of q is thus derived and expressed as

$$q < \frac{1}{6\mu_f} \frac{\tau_a^3}{(\rho_f g)^2} \quad (15)$$

For a given value of τ_a and the value of q satisfying the limit (15), the distribution of film thickness can thus be solved from Eq. (13) with boundary value given by Eq. (14).

From Fig. 4, the shear stress between wall and air is $\tau_a = 1.75 N/m^2$ at shaft speed 8,000 RPM, without the existence of a film. If this value is used as the representative shear stress between air and film, from Eq. (15), the limitation q is $q_{lim} = 9.2816E-7 m^2/s$ for $\tau_a = 1.75 N/m^2$.

To avoid an excessively high value when the denominator in Eq. (13) is approaching zero, a value of $q = 7.8E-7 m^2/s$ is taken. Using the weak convection Eq. (13), the distribution of film thickness can then be solved. The mean value of film thickness is $h = 0.1mm$. For comparison, a Newton's method is also used to solve the steady state depth averaged equation with initial film thickness $h = 0.1mm$ and air shear stress $\tau_a = 1.75 N/m^2$. As shown in Fig. 5, the film thickness distributions obtained from the two approaches are almost identical, providing reassurance to the numerical computations.

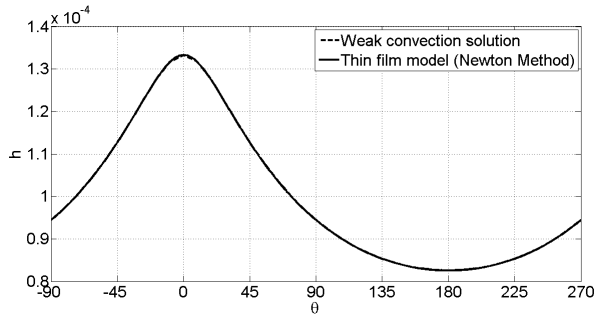


Figure 5. FILM THICKNESS DISTRIBUTIONS PREDICTED BY USING WEAK CONVECTION ASSUMPTION AND SOLVING DEPTH AVERAGED EQUATIONS.

For the experimental data shown in Table 1, the film thickness is about 2mm, and the velocity is about 2m/s, which implies that the weak convection assumption is not valid here. This indicates that using the shear stress value between air and wall as the driving shear stress between air and film may not be appropriate. The value of the air shear stress is therefore taken as $\tau_a = 66.67 N/m^2$ for the following numerical calculations.

Table 1. TYPICAL FILM THICKNESS AND VELOCITY.

| | Karlsruhe Chamber (Wittig & Glahn, 1994) |
|-----------------------|--|
| $h_{ref} (m)$ | 2.1×10^{-3} |
| $\bar{U}_{ref} (m/s)$ | 2.00 |

SIMULATION OF DROPLET IMPINGEMENT

In an engine bearing chamber, the film receives the impact from oil droplets in a dispersed or discrete form. It is usual to calculate the trajectories of droplets in CFD using a Lagrangian framework. Therefore, dealing with the discretized sources from droplet impingement is one natural approach in the thin film calculation: the mass, momentum and energy sources resulting from each droplet impact need to be taken into account in the thin film calculation. Due to the complex nature of the environment in engine bearing chambers, dealing with large droplet impingement on the film is inevitable. In the present paper, three types of droplet impingement models are studied. For comparison purposes, the simulations are using both proposed models (7) and (8) and Chew's models (9) and (10). The profile variation term E_ξ and surface tension S_ξ in Eq. (5) are ignored. To balance the mass in the chamber, a simplified point scavenge is put at the bottom of the chamber and the mass flow through the scavenge is taken equal to the mass of injected oil. This scavenge condition is also a replacement of the term representing the flow crossing over the wall surface V_ξ in Eq. (5).

Single point droplet impingement

It is assumed that a droplet stream continuously impacts on the top point of the simplified chamber with shear velocity $U_{ds} = 5m/s$. Two single point droplet impingement cases are tested: with and without normal-to-film surface impacting velocity $U_{dn} = 5m/s$. According to the formulation in Eq. (8), the pressure term induced by droplet impingement will be active once the droplet normal velocity is considered. The film is initialized as uniform thickness 1mm and velocity 3m/s. Figure 6 shows the film thickness distribution predicted by the proposed model and by Chew's model for single point droplet impingement without normal velocity. Figure 7 shows the film velocity predicted by two models for single point droplet impingement without normal velocity.

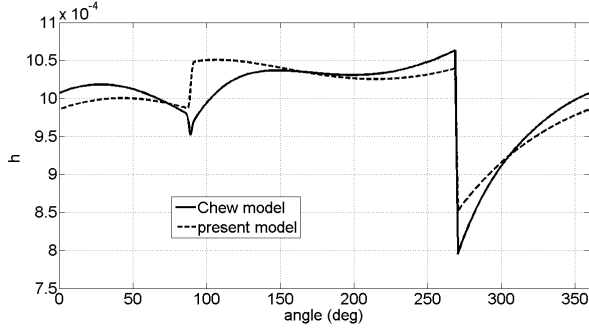


Figure 6. FILM THICKNESS DISTRIBUTIONS PREDICTED BY TWO MODELS FOR SINGLE POINT DROPLET IMPINGEMENT WITHOUT NORMAL VELOCITY.

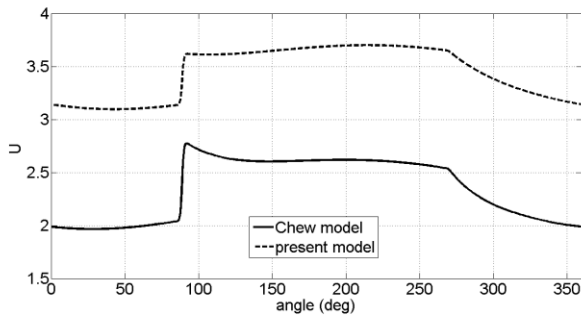


Figure 7. FILM VELOCITY DISTRIBUTIONS PREDICTED BY TWO MODELS FOR SINGLE POINT DROPLET IMPINGEMENT WITHOUT NORMAL VELOCITY.

From Figs. 6 and 7, it can be seen that the film velocity predicted by the proposed model is larger than that predicted by the modified Chew's model. There are two explanations for this. By comparing the wall shear models (7) and (9), it can be seen that there is an extra contribution of air shear in the proposed model, which leads to a higher shear stress contribution than in Chew's model. From Fig. 7, the film velocity is about $\bar{U}_f = 3.1 \sim 3.7 m/s$ with the present model and $\bar{U}_f = 2 \sim 2.7 m/s$ with Chew's model, for an injected droplet shear velocity of $U_{ds} = 5 m/s$. Therefore, the result of droplet impingement is to accelerate the film. By comparing the droplet-film interaction models (8) and (10), there is an extra contribution from shear induced by droplet-film interaction in our model: $0.5(U_{ds} - \bar{U}_f)\dot{m}/\rho_f$. Results show when the injected droplet shear velocity is bigger than local film velocity, the acceleration given in the present model is more than that given by Chew's model.

Figure 8 shows the film thickness distribution predicted by the two models for single space point droplet impingement with normal velocity, and Fig. 9 the film velocity distributions. A

peak in the film solution curve at the droplet impingement point is predicted by the current model which is different from Chew's model. It is believed to be coming from the extra pressure term induced by the droplet impingement in model (8). This phenomenon reflects the "blockage-effect" of normal droplet impingement, which can be captured by the present model.

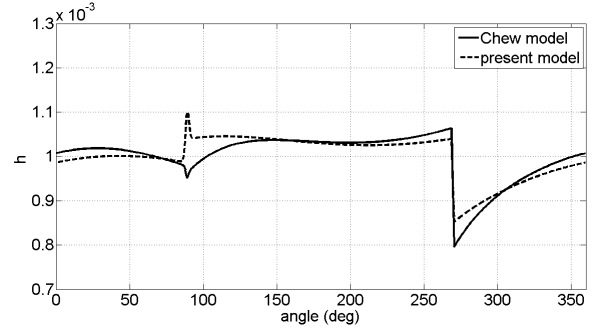


Figure 8. FILM THICKNESS DISTRIBUTIONS PREDICTED BY TWO MODELS FOR SINGLE POINT DROPLET IMPINGEMENT WITH NORMAL VELOCITY.

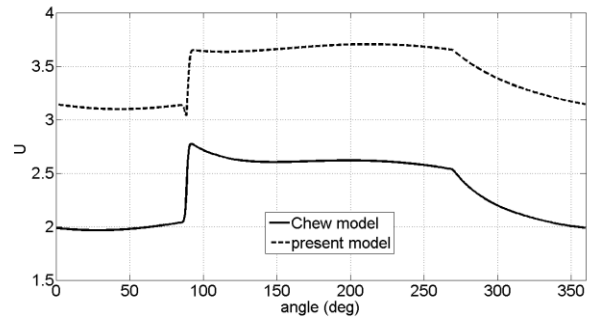


Figure 9. FILM THICKNESS DISTRIBUTIONS PREDICTED BY TWO MODELS FOR SINGLE POINT DROPLET IMPINGEMENT WITH NORMAL VELOCITY.

Random distributed droplet impingement

We consider simulating droplet-film interaction in bearing chambers where the lubricating oil droplets hit the wall randomly and frequently; the droplets are set to impact the film with shear velocity $U_{ds} = 5 m/s$ and normal velocity $U_{dn} = 5 m/s$ at random positions. The film is initialized as uniform thickness 1mm and velocity 3m/s. The resulting film thickness distribution and velocity predicted by the current model and Chew's model are plotted in Figs. 10 and 11.

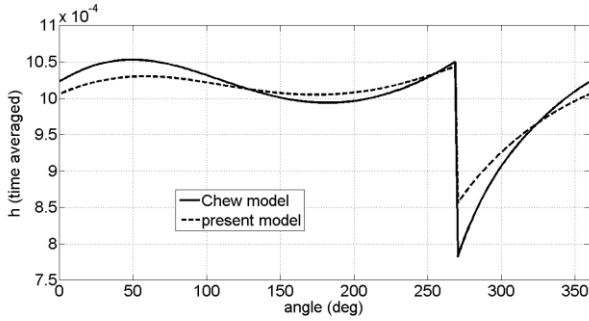


Figure 10. TIME AVERAGED FILM THICKNESS PREDICTED BY TWO MODELS FOR RANDOM DROPLET IMPINGEMENT.

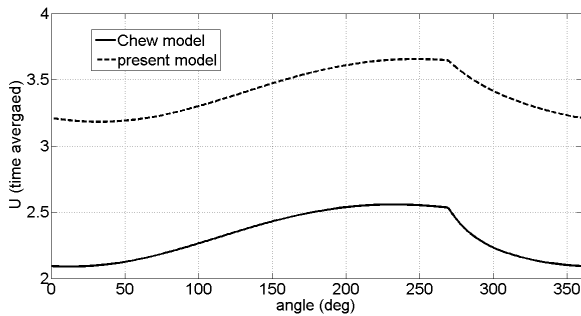


Figure 11. TIME AVERAGED FILM VELOCITY PREDICTED BY TWO MODELS FOR RANDOM DROPLET IMPINGEMENT.

It can be seen that the time averaged film thickness predicted by the two models are quite close, while the velocity predicted by the present model is a little higher, as expected for reasons explained.

A converging strategy

The solution for the random distribution impingement case is obtained by using an unsteady solver and after approximately 200,000 time steps ($\Delta t = 1.E-4s$). Ideally the computation of film flow should be coupled with the solution for the core flow in the real engine bearing chamber CFD simulation. Such a computational cost spent on the film solution alone is not readily acceptable.

An alternative strategy is developed for solving thin film flows:

- Create an intermediate array to hold the time averaged droplet impingement sources from the CFD (Lagrangian).
- Use a steady solver (iterative method or Newton's method) and load the intermediate array created in the previous step to solve film, which would receive a mean representative oil source.

Figure 12 shows the converging histories by plotting the iteration error against time steps or iterations of the various methods. The criterion used to stop the computation is

$\max|\phi^{n+1} - \phi^n| < 10^{-10}$ where n is the iteration number and ϕ is the variable considered. It can be seen that the computation based on the original unsteady approach never reaches the stop criteria. This is because each droplet impact is immediately accounted for in the film calculation which it continuously perturbs. Since the positions of droplet impingement are randomly changing with time, there is indeed never a steady state to be reached. This kind of computation is therefore numerically very costly. The computation based on the iterative steady solver can approach the cancelling criteria after 10^4 iterations, while the computation based on converging strategy mentioned above and coupled to a Newton's method can approach the stop criteria after just 40 iterations.

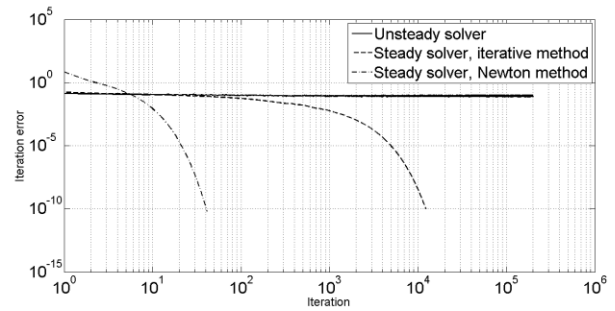


Figure 12. HISTORY OF ITERATION ERRORS RECORDED FROM THREE COMPUTATION APPROACHES.

Figure 13 show the computational results of instantaneous and time averaged film thickness obtained from the unsteady solver against the results obtained from two approaches for steady flow. The time averaged thickness and two steady state solutions are almost identical, which suggested that the given converging strategy is working efficiently.

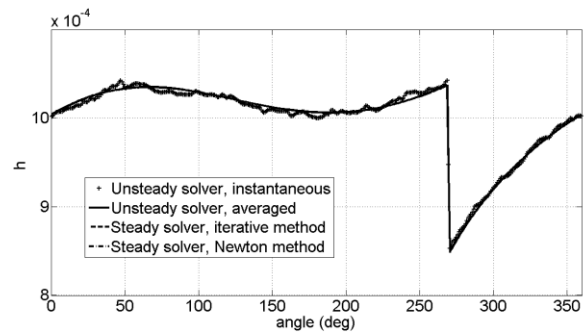


Figure 13. FILM THICKNESS OBTAINED FROM VARIOUS APPROACHES.

CONCLUSION

An air, oil droplet and film interaction model for a bearing chamber environment has been studied numerically. The

physical mechanisms driving the thin film flow are discussed by analyzing the depth averaged mass and momentum equations under thin film assumptions.

A model for the velocity profile over the film depth and a model for droplet-film interaction are needed for the closure of depth averaged governing equations. In the present paper, a quadratic velocity profile is assumed and a new, simple droplet-film interaction models is proposed. The numerical calculations of droplet-film interaction in a simplified bearing chamber model show that these models can capture the main features of the flows and work efficiently. The further validation of proposed model against experimental data, e.g. measured by Gorse et al. [14], is to be made in successive investigation.

By analyzing the thin film flow under weak convection, the relationship between the film mass flux and the air shear stress acting on the film is formulated. It is found that the value of shear stress taken as that at the wall between the wall and the air, ignoring the existence of a film, is not suitable to be used as the air shear stress on the film.

Finally, a useful converging strategy for integrated numerical simulation of engine bearing chamber is given.

ACKNOWLEDGMENTS

The work was partly funded by the European Union within the research project ELUBSYS (Engine Lubrication System Technologies), grant agreement no. ACP8-GA-2009-233651. This financial support is gratefully acknowledged.

The work was also partly funded by Rolls-Royce plc. This financial support is gratefully acknowledged. The authors wish to thank Adrian Jacobs of Rolls-Royce plc for technical support.

NOMENCLATURE

| | |
|-----------------------------|--|
| g, \mathbf{g} | gravity and gravity vector |
| h | film thickness |
| \dot{m} | oil mass flux of droplet-film interaction |
| p | pressure |
| q | Film volume flow rate per unit length |
| R | radius |
| s, y, x | nature coordinates on film-attached wall surface |
| t | time |
| U_{dn} | droplet velocity component (normal to interface) |
| U_{ds} | droplet velocity component (tangential to interface) |
| \mathbf{u} | film velocity vector |
| U, V, W | film velocity components along s, y, x respectively |
| $\bar{U}, \bar{V}, \bar{W}$ | depth averaged film velocity components along s, y, x respectively |
| $\hat{U}, \hat{V}, \hat{W}$ | profile variation of film velocity components along s, y, x respectively |
| \tilde{V} | film surface velocity |
| ρ | density |
| σ | surface tension |
| μ | viscosity |
| τ | shear stress |

η normalized coordinate $\eta = y/h$

Subscripts

| | |
|-----|---|
| a | air |
| d | droplet |
| f | film |
| s | tangential component along s coordinate |
| w | wall |
| x | tangential component along x coordinate |
| y | normal component along y coordinate |

REFERENCES

- [1] Mashayek, F., and Pandya, R. V. R., 2003, "Analytical Description of Particle/droplet-laden Turbulent Flows," *Progress in Energy and Combustion Science*, 29, pp. 329-378.
- [2] Harlow, F., and Welch, J. E., 1965, "Numerical Calculation of Time-Dependent Viscous Incompressible Flow of Fluid with a Free Surface," *Phys. Fluids.*, 8, No. 2182-9.
- [3] Hirt, C. W., and Nichols, B. D., 1981, "Volume of Fluid (VOF) Method for the Dynamics of Free Boundaries," *Journal of Computational Physics*, 39, pp. 201-225.
- [4] Chang, Y. C., Hou, T. Y., Merriman, B., and Osher, S., 1996, "A Level Set Formulation of Eulerian Interface Capturing Methods for Incompressible Fluid Flows," *J. Comput. Phys.*, 124, pp. 449-464.
- [5] Chew, J. W., 1996, "Analysis of the Oil Film on the Inside Surface of an Aero-engine Bearing Chamber," *International Gas Turbine and Aeroengine Congress & Exhibition*, No. 96-GT-300.
- [6] Farral, M., Simmons, K., Hibberd, S., and Gorse, P., 2004, "A Numerical Model for Oil Film Flow in an Aero-engine Bearing Chamber and Comparison with Experimental Data," *Proceedings of ASME Turbo Expo 2004: Power for Lands, Sea and Air*, No. GT2004-53698.
- [7] O'Rourke, P. J., and Amsden, A. A., 1996, "A Particle Numerical Model for Wall Film Dynamics in Port-Injected Engines," *SAE Paper 961961*.
- [8] O'Rourke, P. J., and Amsden, A. A., 2000, "A Spray/wall Interaction Sub model for the KIVA-3 Wall Film Model," *SAE Paper 2000-01-0271*.
- [9] Bai, C., and Gosman, A. D., 1996, "Mathematical Modelling of Wall Films Formed by Impinging Sprays," *SAE paper 960626*.

- [10] Williams, J., 2007, "The Effect of Droplet Impact on Thin Film Rimming Flow," PhD Report, University of Nottingham.
- [11] MATLAB R2010a, 2010, Natick, Massachusetts: The MathWorks Inc.
- [12] Williams, J., 2008, "Thin Film Rimming Flow Subject to Droplet Impact at the Surface," PhD Thesis, University of Nottingham.
- [13] Launder, B. E., and Spalding, D. B., 1974, "The Numerical Computation of Turbulent Flow," Computer Methods in Applied Mechanics and Engineering, 3, pp. 269-289.
- [14] Gorse, P., Busam. and Dullenkopf, K., 2004, "Influence of Operating Condition and Geometry on the Oil Film Thickness in Aero-Engine Bearing Chambers," Proceedings of the ASME Turbo Expo 2004, June 14-17, Vienna, Austria.